

UNIVERSITY OF MANNHEIM

MASTER THESIS

---

# Quasi-Monte Carlo Methods and Neural Networks

---

*Author:*  
Janik V. HRUBANT

*Supervisors:*  
Prof. Dr. Andreas  
NEUENKIRCH

*A thesis submitted in fulfillment of the requirements  
for the degree of Master of Science  
in the*

Research Group Name  
Department or School Name

July 15, 2025



## Declaration of Authorship

I, Janik V. HRUBANT, declare that this thesis titled, "Quasi-Monte Carlo Methods and Neural Networks" and the work presented in it are my own. I confirm that:

- This work was done wholly or mainly while in candidature for a research degree at this University.
- Where any part of this thesis has previously been submitted for a degree or any other qualification at this University or any other institution, this has been clearly stated.
- Where I have consulted the published work of others, this is always clearly attributed.
- Where I have quoted from the work of others, the source is always given. With the exception of such quotations, this thesis is entirely my own work.
- I have acknowledged all main sources of help.
- Where the thesis is based on work done by myself jointly with others, I have made clear exactly what was done by others and what I have contributed myself.

Signed:

Date:



## *Abstract*

This thesis explores the application of quasi-Monte Carlo (QMC) methods for generating training data for neural networks, with a particular emphasis on convergence behavior in both deterministic and stochastic settings. In contrast to classical Monte Carlo (MC) approaches, which rely on pseudorandom sampling, QMC methods use low-discrepancy sequences to achieve more uniform coverage of the input space, which can lead to improved approximation performance, especially in high-dimensional problems.

In the first part of the thesis, QMC methods are applied to sample training inputs from a bounded domain. The corresponding function values are computed, and the resulting dataset is used to train neural networks. The convergence of the network output with respect to the number of training points is analyzed and compared against networks trained on MC-sampled data. The goal is to quantify the advantage of QMC-based training in terms of learning efficiency and approximation accuracy.

The second part extends this investigation to stochastic functions. Here, the randomness in the system—such as in photon transport models—is explicitly modeled, and both QMC and MC sampling are used to sample from the stochastic variables. The focus is on physically motivated functions that simulate scattered photon radiation, a key challenge in medical imaging applications such as x-ray or CT simulations. Neural networks are trained on data generated from these stochastic models, and their convergence behavior is evaluated under QMC and MC sampling regimes.

Through these experiments, the thesis demonstrates how QMC-based sampling can enhance neural network training, particularly when approximating complex physical processes. The results provide both theoretical insights and empirical evidence that QMC methods offer significant advantages over standard MC approaches in terms of convergence speed and generalization quality in high-dimensional learning problems.



# Contents

<b>Declaration of Authorship</b>	<b>iii</b>
<b>Abstract</b>	<b>v</b>
<b>I QMC for training of Neural Networks</b>	<b>1</b>
<b>1 Quasi-Monte Carlo Methods for Deep Learning: Motivation and Objectives</b>	<b>3</b>
1.1 Challenges in Neural Network Training . . . . .	3
1.2 Limitations of Monte Carlo Sampling . . . . .	3
1.3 Objectives and Scope of the Thesis . . . . .	3
1.4 Outline of the Thesis . . . . .	4
<b>2 Theoretical Foundations</b>	<b>5</b>
2.1 Function Approximation with Neural Networks . . . . .	5
2.2 Sampling-Based Learning: MC vs. QMC . . . . .	5
2.2.1 Monte Carlo Sampling in High Dimensions . . . . .	5
2.2.2 Low-Discrepancy Sequences and QMC Theory . . . . .	5
2.3 Convergence in Deterministic and Stochastic Learning . . . . .	6
2.4 Stochastic Functions and Photon Transport Models . . . . .	6
<b>3 Neural Network Training with QMC in Deterministic Settings</b>	<b>7</b>
3.1 Problem Setup and Input Space Design . . . . .	7
3.2 Generation of Training Sets via QMC and MC . . . . .	7
3.3 Network Architecture and Training Protocols . . . . .	7
3.4 Convergence Evaluation and Error Metrics . . . . .	8
3.5 Comparative Results . . . . .	8
<b>4 Neural Network Training for Stochastic Functions</b>	<b>9</b>
4.1 Modeling Randomness in Physical Simulations . . . . .	9
4.2 Sampling Stochastic Variables with QMC and MC . . . . .	9
4.3 Data Generation: Simulating Photon Scatter . . . . .	9
4.4 Learning Setup and Experimental Design . . . . .	10
4.5 Convergence and Performance Comparison . . . . .	10
<b>II X-ray Simulation using QMC Methods</b>	<b>11</b>
<b>5 Motivation and Problem Statement</b>	<b>13</b>
5.1 Computed Tomography Imaging . . . . .	13
5.2 X-ray Imaging and the Challenge of Scatter . . . . .	13

5.3	Scatter Correction Methods for X-ray Imaging . . . . .	14
5.3.1	Overview of Scatter Correction Techniques . . . . .	14
5.3.2	Monte Carlo Simulation . . . . .	15
5.4	High-Level Overview of the Monte Carlo Simulation . . . . .	16
5.5	Monte Carlo Methods: Benefits & Drawbacks . . . . .	17
<b>6</b>	<b>Physical laws of Photon Simulation</b>	<b>19</b>
6.1	X-Ray Tube . . . . .	20
6.1.1	Photon Generation . . . . .	20
6.1.2	Filter . . . . .	23
6.2	Photon Generation . . . . .	24
6.3	Scattering and Attenuation . . . . .	25
6.3.1	Free Path Length . . . . .	26
6.3.2	Compton Scattering . . . . .	28
6.3.3	Rayleigh Scattering . . . . .	28
<b>7</b>	<b>The Simulation Algorithm</b>	<b>31</b>
7.1	Algorithm overview . . . . .	31
7.2	Sub-Algorithms . . . . .	31
7.2.1	Photon Generation . . . . .	31
<b>A</b>	<b>Frequently Asked Questions</b>	<b>37</b>
A.1	How do I change the colors of links? . . . . .	37
<b>Bibliography</b>		<b>39</b>

**RITA** Rational Inverse Transform with Aliasing

**CDF** Cumulative Distribution Function

**QMC** Quasi-Monte Carlo

**MC** Monte Carlo

**HU** Hounsfield Unit

**CT** Computed Tomography

**CBCT** Cone-Beam Computed Tomography

**FFD** Forced Fixed Detection



## Part I

# QMC for training of Neural Networks



## Chapter 1

# Quasi-Monte Carlo Methods for Deep Learning: Motivation and Objectives

### 1.1 Challenges in Neural Network Training

Lorem ipsum dolor sit amet, consectetur adipiscing elit. Aliquam ultricies lacinia euismod. Nam tempus risus in dolor rhoncus in interdum enim tincidunt. Donec vel nunc neque. In condimentum ullamcorper quam non consequat. Fusce sagittis tempor feugiat. Fusce magna erat, molestie eu convallis ut, tempus sed arcu. Quisque molestie, ante a tincidunt ullamcorper, sapien enim dignissim lacus, in semper nibh erat lobortis purus. Integer dapibus ligula ac risus convallis pellentesque.

### 1.2 Limitations of Monte Carlo Sampling

Sed ullamcorper quam eu nisl interdum at interdum enim egestas. Aliquam placerat justo sed lectus lobortis ut porta nisl porttitor. Vestibulum mi dolor, lacinia molestie gravida at, tempus vitae ligula. Donec eget quam sapien, in viverra eros. Donec pellentesque justo a massa fringilla non vestibulum metus vestibulum. Vestibulum in orci quis felis tempor lacinia. Vivamus ornare ultrices facilisis. Ut hendrerit volutpat vulputate. Morbi condimentum venenatis augue, id porta ipsum vulputate in. Curabitur luctus tempus justo. Vestibulum risus lectus, adipiscing nec condimentum quis, condimentum nec nisl. Aliquam dictum sagittis velit sed iaculis. Morbi tristique augue sit amet nulla pulvinar id facilisis ligula mollis. Nam elit libero, tincidunt ut aliquam at, molestie in quam. Aenean rhoncus vehicula hendrerit.

### 1.3 Objectives and Scope of the Thesis

Sed ullamcorper quam eu nisl interdum at interdum enim egestas. Aliquam placerat justo sed lectus lobortis ut porta nisl porttitor. Vestibulum mi dolor, lacinia molestie gravida at, tempus vitae ligula. Donec eget quam sapien, in viverra eros. Donec pellentesque justo a massa fringilla non vestibulum metus vestibulum. Vestibulum in orci quis felis tempor lacinia. Vivamus ornare ultrices facilisis. Ut hendrerit volutpat vulputate. Morbi condimentum venenatis augue, id porta ipsum vulputate in. Curabitur luctus tempus justo. Vestibulum risus lectus, adipiscing nec condimentum quis, condimentum nec nisl. Aliquam dictum sagittis velit sed iaculis. Morbi

tristique augue sit amet nulla pulvinar id facilisis ligula mollis. Nam elit libero, tinidunt ut aliquam at, molestie in quam. Aenean rhoncus vehicula hendrerit.

## 1.4 Outline of the Thesis

Sed ullamcorper quam eu nisl interdum at interdum enim egestas. Aliquam placerat justo sed lectus lobortis ut porta nisl porttitor. Vestibulum mi dolor, lacinia molestie gravida at, tempus vitae ligula. Donec eget quam sapien, in viverra eros. Donec pellentesque justo a massa fringilla non vestibulum metus vestibulum. Vestibulum in orci quis felis tempor lacinia. Vivamus ornare ultrices facilisis. Ut hendrerit volutpat vulputate. Morbi condimentum venenatis augue, id porta ipsum vulputate in. Curabitur luctus tempus justo. Vestibulum risus lectus, adipiscing nec condimentum quis, condimentum nec nisl. Aliquam dictum sagittis velit sed iaculis. Morbi tristique augue sit amet nulla pulvinar id facilisis ligula mollis. Nam elit libero, tinidunt ut aliquam at, molestie in quam. Aenean rhoncus vehicula hendrerit.

## Chapter 2

# Theoretical Foundations

### 2.1 Function Approximation with Neural Networks

Lorem ipsum dolor sit amet, consectetur adipiscing elit. Aliquam ultricies lacinia euismod. Nam tempus risus in dolor rhoncus in interdum enim tincidunt. Donec vel nunc neque. In condimentum ullamcorper quam non consequat. Fusce sagittis tempor feugiat. Fusce magna erat, molestie eu convallis ut, tempus sed arcu. Quisque molestie, ante a tincidunt ullamcorper, sapien enim dignissim lacus, in semper nibh erat lobortis purus. Integer dapibus ligula ac risus convallis pellentesque.

### 2.2 Sampling-Based Learning: MC vs. QMC

Lorem ipsum dolor sit amet, consectetur adipiscing elit. Aliquam ultricies lacinia euismod. Nam tempus risus in dolor rhoncus in interdum enim tincidunt. Donec vel nunc neque. In condimentum ullamcorper quam non consequat. Fusce sagittis tempor feugiat. Fusce magna erat, molestie eu convallis ut, tempus sed arcu. Quisque molestie, ante a tincidunt ullamcorper, sapien enim dignissim lacus, in semper nibh erat lobortis purus. Integer dapibus ligula ac risus convallis pellentesque.

#### 2.2.1 Monte Carlo Sampling in High Dimensions

Nunc posuere quam at lectus tristique eu ultrices augue venenatis. Vestibulum ante ipsum primis in faucibus orci luctus et ultrices posuere cubilia Curae; Aliquam erat volutpat. Vivamus sodales tortor eget quam adipiscing in vulputate ante ullamcorper. Sed eros ante, lacinia et sollicitudin et, aliquam sit amet augue. In hac habitasse platea dictumst.

#### 2.2.2 Low-Discrepancy Sequences and QMC Theory

Morbi rutrum odio eget arcu adipiscing sodales. Aenean et purus a est pulvinar pellentesque. Cras in elit neque, quis varius elit. Phasellus fringilla, nibh eu tempus venenatis, dolor elit posuere quam, quis adipiscing urna leo nec orci. Sed nec nulla auctor odio aliquet consequat. Ut nec nulla in ante ullamcorper aliquam at sed dolor. Phasellus fermentum magna in augue gravida cursus. Cras sed pretium lorem. Pellentesque eget ornare odio. Proin accumsan, massa viverra cursus pharetra, ipsum nisi lobortis velit, a malesuada dolor lorem eu neque.

## 2.3 Convergence in Deterministic and Stochastic Learning

Sed ullamcorper quam eu nisl interdum at interdum enim egestas. Aliquam placerat justo sed lectus lobortis ut porta nisl porttitor. Vestibulum mi dolor, lacinia molestie gravida at, tempus vitae ligula. Donec eget quam sapien, in viverra eros. Donec pellentesque justo a massa fringilla non vestibulum metus vestibulum. Vestibulum in orci quis felis tempor lacinia. Vivamus ornare ultrices facilisis. Ut hendrerit volutpat vulputate. Morbi condimentum venenatis augue, id porta ipsum vulputate in. Curabitur luctus tempus justo. Vestibulum risus lectus, adipiscing nec condimentum quis, condimentum nec nisl. Aliquam dictum sagittis velit sed iaculis. Morbi tristique augue sit amet nulla pulvinar id facilisis ligula mollis. Nam elit libero, tincidunt ut aliquam at, molestie in quam. Aenean rhoncus vehicula hendrerit.

## 2.4 Stochastic Functions and Photon Transport Models

Sed ullamcorper quam eu nisl interdum at interdum enim egestas. Aliquam placerat justo sed lectus lobortis ut porta nisl porttitor. Vestibulum mi dolor, lacinia molestie gravida at, tempus vitae ligula. Donec eget quam sapien, in viverra eros. Donec pellentesque justo a massa fringilla non vestibulum metus vestibulum. Vestibulum in orci quis felis tempor lacinia. Vivamus ornare ultrices facilisis. Ut hendrerit volutpat vulputate. Morbi condimentum venenatis augue, id porta ipsum vulputate in. Curabitur luctus tempus justo. Vestibulum risus lectus, adipiscing nec condimentum quis, condimentum nec nisl. Aliquam dictum sagittis velit sed iaculis. Morbi tristique augue sit amet nulla pulvinar id facilisis ligula mollis. Nam elit libero, tincidunt ut aliquam at, molestie in quam. Aenean rhoncus vehicula hendrerit.

## Chapter 3

# Neural Network Training with QMC in Deterministic Settings

### 3.1 Problem Setup and Input Space Design

Lorem ipsum dolor sit amet, consectetur adipiscing elit. Aliquam ultricies lacinia euismod. Nam tempus risus in dolor rhoncus in interdum enim tincidunt. Donec vel nunc neque. In condimentum ullamcorper quam non consequat. Fusce sagittis tempor feugiat. Fusce magna erat, molestie eu convallis ut, tempus sed arcu. Quisque molestie, ante a tincidunt ullamcorper, sapien enim dignissim lacus, in semper nibh erat lobortis purus. Integer dapibus ligula ac risus convallis pellentesque.

### 3.2 Generation of Training Sets via QMC and MC

Sed ullamcorper quam eu nisl interdum at interdum enim egestas. Aliquam placerat justo sed lectus lobortis ut porta nisl porttitor. Vestibulum mi dolor, lacinia molestie gravida at, tempus vitae ligula. Donec eget quam sapien, in viverra eros. Donec pellentesque justo a massa fringilla non vestibulum metus vestibulum. Vestibulum in orci quis felis tempor lacinia. Vivamus ornare ultrices facilisis. Ut hendrerit volutpat vulputate. Morbi condimentum venenatis augue, id porta ipsum vulputate in. Curabitur luctus tempus justo. Vestibulum risus lectus, adipiscing nec condimentum quis, condimentum nec nisl. Aliquam dictum sagittis velit sed iaculis. Morbi tristique augue sit amet nulla pulvinar id facilisis ligula mollis. Nam elit libero, tincidunt ut aliquam at, molestie in quam. Aenean rhoncus vehicula hendrerit.

### 3.3 Network Architecture and Training Protocols

Sed ullamcorper quam eu nisl interdum at interdum enim egestas. Aliquam placerat justo sed lectus lobortis ut porta nisl porttitor. Vestibulum mi dolor, lacinia molestie gravida at, tempus vitae ligula. Donec eget quam sapien, in viverra eros. Donec pellentesque justo a massa fringilla non vestibulum metus vestibulum. Vestibulum in orci quis felis tempor lacinia. Vivamus ornare ultrices facilisis. Ut hendrerit volutpat vulputate. Morbi condimentum venenatis augue, id porta ipsum vulputate in. Curabitur luctus tempus justo. Vestibulum risus lectus, adipiscing nec condimentum quis, condimentum nec nisl. Aliquam dictum sagittis velit sed iaculis. Morbi tristique augue sit amet nulla pulvinar id facilisis ligula mollis. Nam elit libero, tincidunt ut aliquam at, molestie in quam. Aenean rhoncus vehicula hendrerit.

## 3.4 Convergence Evaluation and Error Metrics

Sed ullamcorper quam eu nisl interdum at interdum enim egestas. Aliquam placerat justo sed lectus lobortis ut porta nisl porttitor. Vestibulum mi dolor, lacinia molestie gravida at, tempus vitae ligula. Donec eget quam sapien, in viverra eros. Donec pellentesque justo a massa fringilla non vestibulum metus vestibulum. Vestibulum in orci quis felis tempor lacinia. Vivamus ornare ultrices facilisis. Ut hendrerit volutpat vulputate. Morbi condimentum venenatis augue, id porta ipsum vulputate in. Curabitur luctus tempus justo. Vestibulum risus lectus, adipiscing nec condimentum quis, condimentum nec nisl. Aliquam dictum sagittis velit sed iaculis. Morbi tristique augue sit amet nulla pulvinar id facilisis ligula mollis. Nam elit libero, tincidunt ut aliquam at, molestie in quam. Aenean rhoncus vehicula hendrerit.

## 3.5 Comparative Results

Sed ullamcorper quam eu nisl interdum at interdum enim egestas. Aliquam placerat justo sed lectus lobortis ut porta nisl porttitor. Vestibulum mi dolor, lacinia molestie gravida at, tempus vitae ligula. Donec eget quam sapien, in viverra eros. Donec pellentesque justo a massa fringilla non vestibulum metus vestibulum. Vestibulum in orci quis felis tempor lacinia. Vivamus ornare ultrices facilisis. Ut hendrerit volutpat vulputate. Morbi condimentum venenatis augue, id porta ipsum vulputate in. Curabitur luctus tempus justo. Vestibulum risus lectus, adipiscing nec condimentum quis, condimentum nec nisl. Aliquam dictum sagittis velit sed iaculis. Morbi tristique augue sit amet nulla pulvinar id facilisis ligula mollis. Nam elit libero, tincidunt ut aliquam at, molestie in quam. Aenean rhoncus vehicula hendrerit.

## Chapter 4

# Neural Network Training for Stochastic Functions

### 4.1 Modeling Randomness in Physical Simulations

Lorem ipsum dolor sit amet, consectetur adipiscing elit. Aliquam ultricies lacinia euismod. Nam tempus risus in dolor rhoncus in interdum enim tincidunt. Donec vel nunc neque. In condimentum ullamcorper quam non consequat. Fusce sagittis tempor feugiat. Fusce magna erat, molestie eu convallis ut, tempus sed arcu. Quisque molestie, ante a tincidunt ullamcorper, sapien enim dignissim lacus, in semper nibh erat lobortis purus. Integer dapibus ligula ac risus convallis pellentesque.

### 4.2 Sampling Stochastic Variables with QMC and MC

Sed ullamcorper quam eu nisl interdum at interdum enim egestas. Aliquam placerat justo sed lectus lobortis ut porta nisl porttitor. Vestibulum mi dolor, lacinia molestie gravida at, tempus vitae ligula. Donec eget quam sapien, in viverra eros. Donec pellentesque justo a massa fringilla non vestibulum metus vestibulum. Vestibulum in orci quis felis tempor lacinia. Vivamus ornare ultrices facilisis. Ut hendrerit volutpat vulputate. Morbi condimentum venenatis augue, id porta ipsum vulputate in. Curabitur luctus tempus justo. Vestibulum risus lectus, adipiscing nec condimentum quis, condimentum nec nisl. Aliquam dictum sagittis velit sed iaculis. Morbi tristique augue sit amet nulla pulvinar id facilisis ligula mollis. Nam elit libero, tincidunt ut aliquam at, molestie in quam. Aenean rhoncus vehicula hendrerit.

### 4.3 Data Generation: Simulating Photon Scatter

Sed ullamcorper quam eu nisl interdum at interdum enim egestas. Aliquam placerat justo sed lectus lobortis ut porta nisl porttitor. Vestibulum mi dolor, lacinia molestie gravida at, tempus vitae ligula. Donec eget quam sapien, in viverra eros. Donec pellentesque justo a massa fringilla non vestibulum metus vestibulum. Vestibulum in orci quis felis tempor lacinia. Vivamus ornare ultrices facilisis. Ut hendrerit volutpat vulputate. Morbi condimentum venenatis augue, id porta ipsum vulputate in. Curabitur luctus tempus justo. Vestibulum risus lectus, adipiscing nec condimentum quis, condimentum nec nisl. Aliquam dictum sagittis velit sed iaculis. Morbi tristique augue sit amet nulla pulvinar id facilisis ligula mollis. Nam elit libero, tincidunt ut aliquam at, molestie in quam. Aenean rhoncus vehicula hendrerit.

## 4.4 Learning Setup and Experimental Design

Sed ullamcorper quam eu nisl interdum at interdum enim egestas. Aliquam placerat justo sed lectus lobortis ut porta nisl porttitor. Vestibulum mi dolor, lacinia molestie gravida at, tempus vitae ligula. Donec eget quam sapien, in viverra eros. Donec pellentesque justo a massa fringilla non vestibulum metus vestibulum. Vestibulum in orci quis felis tempor lacinia. Vivamus ornare ultrices facilisis. Ut hendrerit volutpat vulputate. Morbi condimentum venenatis augue, id porta ipsum vulputate in. Curabitur luctus tempus justo. Vestibulum risus lectus, adipiscing nec condimentum quis, condimentum nec nisl. Aliquam dictum sagittis velit sed iaculis. Morbi tristique augue sit amet nulla pulvinar id facilisis ligula mollis. Nam elit libero, tincidunt ut aliquam at, molestie in quam. Aenean rhoncus vehicula hendrerit.

## 4.5 Convergence and Performance Comparison

Sed ullamcorper quam eu nisl interdum at interdum enim egestas. Aliquam placerat justo sed lectus lobortis ut porta nisl porttitor. Vestibulum mi dolor, lacinia molestie gravida at, tempus vitae ligula. Donec eget quam sapien, in viverra eros. Donec pellentesque justo a massa fringilla non vestibulum metus vestibulum. Vestibulum in orci quis felis tempor lacinia. Vivamus ornare ultrices facilisis. Ut hendrerit volutpat vulputate. Morbi condimentum venenatis augue, id porta ipsum vulputate in. Curabitur luctus tempus justo. Vestibulum risus lectus, adipiscing nec condimentum quis, condimentum nec nisl. Aliquam dictum sagittis velit sed iaculis. Morbi tristique augue sit amet nulla pulvinar id facilisis ligula mollis. Nam elit libero, tincidunt ut aliquam at, molestie in quam. Aenean rhoncus vehicula hendrerit.

## Part II

# X-ray Simulation using QMC Methods



## Chapter 5

# Motivation and Problem Statement

### 5.1 Computed Tomography Imaging

Computed Tomography (**CT**) imaging is a powerful medical imaging technique that provides detailed cross-sectional images of a body by combining multiple X-ray projections taken from different angles. This technique is widely used for diagnostic purposes, allowing clinicians to visualize internal structures with high spatial resolution.

The process involves rotating an X-ray source around the patient while simultaneously capturing X-ray projections on a detector array. Each projection represents the cumulative attenuation of X-rays as they pass through various tissues, which is influenced by the density and composition of the materials they encounter.

The collected data is then reconstructed into a three-dimensional volume using sophisticated algorithms, such as filtered backprojection or iterative reconstruction methods. These algorithms convert the raw projection data into cross-sectional images, which can be further processed to enhance contrast, reduce noise and improve overall image quality.

To achieve accurate reconstructions, it is crucial to have precise and high-quality X-ray images. However, one of the most significant challenges in CT imaging is the presence of scattered radiation, which can lead to artifacts and distortions in the reconstructed images.

Throughout this thesis, the term *scatter reduction in CT* refers to the mitigation of scatter-induced artifacts in the 2D X-ray projection images acquired by the detector array during a CT scan. These projections serve as the input for reconstructing the final 3D volume. Given the complexity of the full reconstruction process, the focus of this work will be limited to analyzing and correcting scatter effects at the level of the 2D projection data.

### 5.2 X-ray Imaging and the Challenge of Scatter

X-ray **CT** relies on measuring the attenuation of X-ray photons as they traverse straight-line paths through a phantom. These trajectories typically extend from an X-ray source  $S$  to a detector element  $\mathcal{D}_j$ , forming the path:

$$l = \overrightarrow{SD_j}$$

Under idealized conditions, the attenuation process is governed by the Lambert-Beer law, which describes an exponential decay in intensity as the beam interacts with the material. As stated in [2, Chap. 7], this relationship is given by

$$I = \int_0^{E_{\max}} I_0(E) \cdot \exp \left( - \int_S^{\mathcal{D}_j} \mu(x, E) dx \right) dE \quad (5.1)$$

where  $I_0(E)$  denotes the incident intensity of X-rays with energy  $E$  at source  $S$ . Further  $\mu(x, E)$  represents the linear attenuation coefficient of a photon at any spatial location  $x$  along the path  $l$  with energy  $E$ . The resulting intensity  $I$  is measured at the detector element  $\mathcal{D}_j$ .

Although exponential attenuation along straight-line paths is the idealized model for X-ray imaging, this assumption is systematically violated in practice. As X-rays traverse the scanned object, many photons undergo scattering interactions - such as Compton or Rayleigh scattering - which alter their trajectories. Despite deviating from the primary path, these scattered photons may still reach the detector, adding unintended signal components. As a result, the measured intensities no longer represent pure line integrals of the attenuation map. This discrepancy introduces non-linear errors and visible artifacts in the reconstructed image, ultimately degrading both visual quality and quantitative accuracy.

Scattered radiation is a major source of image artifacts - such as cupping and streaks - and reduces both spatial and contrast resolution. These effects not only degrade visual image quality but also compromise the accuracy of quantitative measurements, such as Hounsfield units  $\mu_*$  [2, Chap. 8], which are used for clinical interpretation such as tissue characterization. Hounsfield units are representing a normalized attenuation to the attenuation of water.

$$\mu_* = \left( \frac{\mu}{\mu_{\text{water}}} - 1 \right) \cdot 1000$$

The impact of scatter becomes especially pronounced in modern CT systems using high-energy X-rays or large-area flat-panel detectors, where scatter may dominate the measured signal. As such, accurate modeling and correction of scatter is essential for achieving high-fidelity CT images, particularly in clinical applications where precision and reliability are paramount [2].

## 5.3 Scatter Correction Methods for X-ray Imaging

### 5.3.1 Overview of Scatter Correction Techniques

In CT, scattered photons are a major source of image artifacts and quantitative inaccuracies. To mitigate these effects, a range of computational scatter correction methods has been developed. These approaches can be broadly classified into the following categories:

- **Empirical and Analytical Methods:**

These include techniques such as primary modulation, convolution-based correction and energy windowing. Scatter is typically estimated using simplified models or empirical kernels, often assuming a smooth background distribution and then subtracted from the measured signal. While computationally

efficient, these methods rely on assumptions regarding the spatial and energy distribution of scattered photons. As a result, they may fail to accurately model complex scatter phenomena in heterogeneous anatomical structures.

- **Physics-Based Models:**

These methods aim to provide a more accurate representation of the underlying photon transport physics, including scattering phenomena. Among them, Monte Carlo (MC) simulation is regarded as the most rigorous and comprehensive technique due to its ability to statistically model complex photon interactions without relying on simplifying assumptions. In such models, primary and scattered photon contributions are simulated separately, allowing the estimated scatter signal to be subtracted from measured data in order to restore image fidelity.

- **TODO: AI Method from Joshua Maier?**

In 2011 Sisniega et al. [7] already demonstrated promising results using the computationally expensive Monte Carlo (MC) simulation of the CT of a cylinder phantom with two bone inserts. The results show significant improvements in the image quality as demonstrated by Sisniega et al. in Figure 5.1.

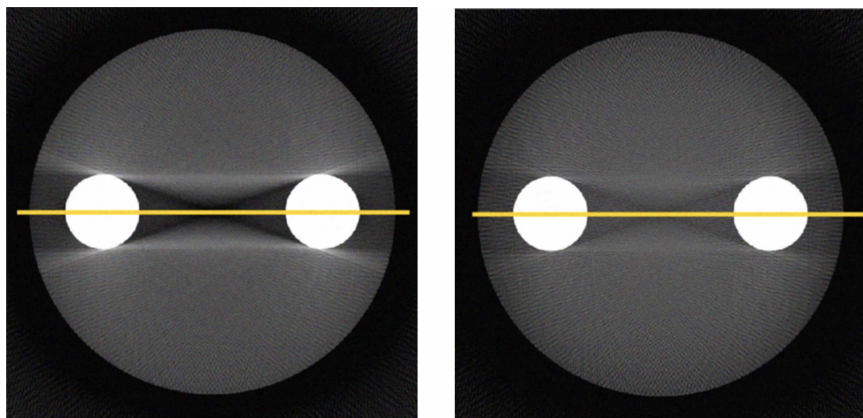


FIGURE 5.1: Cone-Beam Computed Tomography (CBCT) of a 70 mm soft-tissue cylinder with two bone inserts. Left: Image after scatter correction using the gMCFFD method ( $5e6$  photons), showing improved uniformity and quantitative accuracy. Right: Image without correction, exhibiting typical cupping and streak artifacts. (from [7])

### 5.3.2 Monte Carlo Simulation

The MC simulation is a powerful computational technique that follows physics-based principles to model the transport of photons through matter. It is widely recognized as the gold standard for scatter correction in CT and related imaging modalities. This status is attributed to several key factors:

- **Physical Accuracy:**

MC methods simulate the stochastic nature of photon interactions (including Compton and Rayleigh scattering, photoelectric absorption and multiple scattering events) based on fundamental physical cross-sections and material properties.

- **Comprehensive Modeling:**

Unlike analytical or empirical methods, MC simulation can account for complex geometries, heterogeneous materials and realistic X-ray spectra, providing highly accurate estimates of the scatter signal.

- **Validation Benchmark:**

Due to their accuracy, MC-based scatter estimates are routinely used as reference standards for validating and benchmarking faster, approximate correction methods.

## 5.4 High-Level Overview of the Monte Carlo Simulation

Monte Carlo simulation of photon transport for scatter correction involves the following key steps [7]:

1. **Photon Emission:**

Photons are emitted from a virtual X-ray source, with energies sampled from the source spectrum.

2. **Photon Tracking:**

Each photon is tracked as it propagates through the object. At each step, the probability of interaction (scattering or absorption) is determined by the local material properties and cross-sections.

3. **Interaction Sampling:**

When an interaction occurs, the type (e.g., Compton, Rayleigh or Absorption) and the resulting change in photon direction and energy are sampled from the relevant probability distributions.

4. **Detection:**

Photons that reach the detector (either unscattered or after one or more scatter events) are recorded. The simulation keeps track of both primary and scattered photons, allowing for the estimation of the scatter contribution to each detector element.

5. **Statistical Averaging:**

By simulating a large number of photons the method builds up a statistical robust estimate of the scatter distribution. The accuracy of the result increases with the number of simulated photons and eventually converges to a stable intensity distribution.

The schematic flow of the Monte Carlo simulation process is illustrated in Figure 5.2.

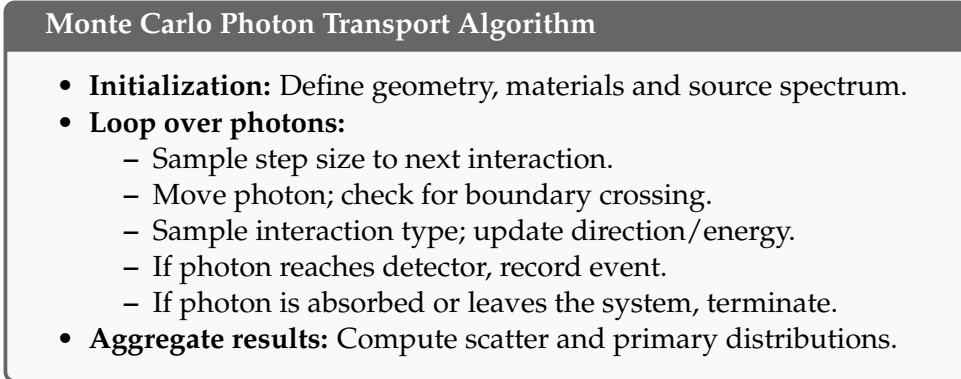


FIGURE 5.2: Pseudocode for photon transport simulation in Monte Carlo scatter modeling.

## 5.5 Monte Carlo Methods: Benefits & Drawbacks

QMC still does not appear in the caption

Monte Carlo (MC) simulations are widely regarded as the gold standard for scatter correction in computed tomography due to their ability to model photon-matter interactions from first principles. These simulations faithfully reproduce all relevant physical scattering phenomena - including Compton and Rayleigh scattering - and can accommodate arbitrarily complex object geometries and heterogeneous material compositions. Owing to this high level of physical realism, MC-based methods yield highly accurate scatter estimates and are therefore commonly used as a reference benchmark for evaluating and validating alternative correction approaches.

However, the high accuracy of Monte Carlo simulations comes at the cost of substantial computational demand. Achieving low-noise scatter estimates requires simulating a large number of photon histories to ensure statistical convergence. As a result, the runtime scales with the desired level of accuracy and can span from several minutes to multiple hours or even days, depending on the complexity of the problem and the available computational resources. This computational burden poses a major practical limitation, particularly in scenarios involving large datasets or iterative reconstruction workflows.

In response to the computational burden of slow converging traditional Monte Carlo methods, recent research has focused on approaches to accelerate this type of precisely correct photon transport simulations. Among these, the application Quasi-Monte Carlo (QMC) methods has gained increasing attention. By replacing random sampling with deterministic low-discrepancy sequences, QMC techniques achieve significantly faster convergence while maintaining comparable accuracy. Contemporary QMC-based scatter correction algorithms have demonstrated runtime reductions of one to two orders of magnitude, thereby enabling high-fidelity simulations even in time-sensitive or resource-constrained settings [1].



## Chapter 6

# Physical laws of Photon Simulation

This chapter introduces the physical and mathematical principles underlying the simulation of X-ray imaging. Central to this is the modeling of individual photon interactions with matter, including attenuation and scattering processes. These interactions are inherently stochastic due to the quantum nature of radiation-matter interactions. The stochastic nature of photons and their interactions with matter is modelled using monte Carlo methods of uniformly distributed values between 0 and 1, which are then transformed to follow the physical probability distributions relevant to the specific interactions being simulated. This approach allows for a realistic representation of photon transport and interaction within the imaging system.

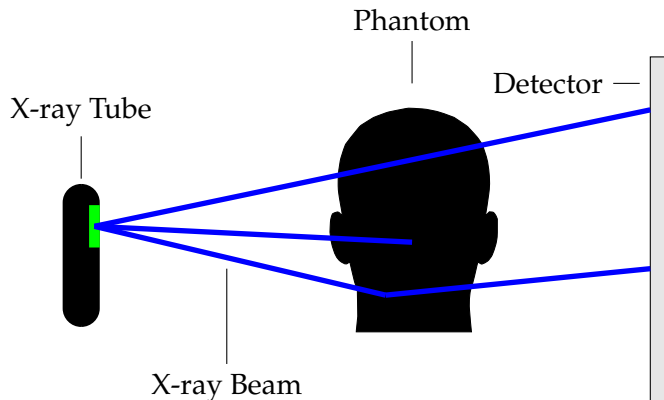


FIGURE 6.1: Schematic illustration of photon transport in X-ray imaging.

In a typical simulation workflow, individual photons are emitted from the X-ray tube and propagate through air before reaching the phantom. Upon entering the phantom, they may interact with the material through scattering or absorption, depending on the local composition of the tissue and photon energy. Only a fraction of the photons will exit the phantom, continue their path through air, and ultimately reach the detector, contributing to the final image formation.

The simulation framework described here forms the basis for all subsequent analyses presented in this thesis.

## 6.1 X-Ray Tube

X-ray beams are generated within evacuated glass tubes containing several critical components that convert electrical energy into X-ray photons and heat. The X-ray tube acts as an energy converter, where the vast majority of the input energy is transformed into heat and only a small fraction becomes useful radiation. The following Figure 6.2 illustrates the basic construction of an X-ray tube as in [5]

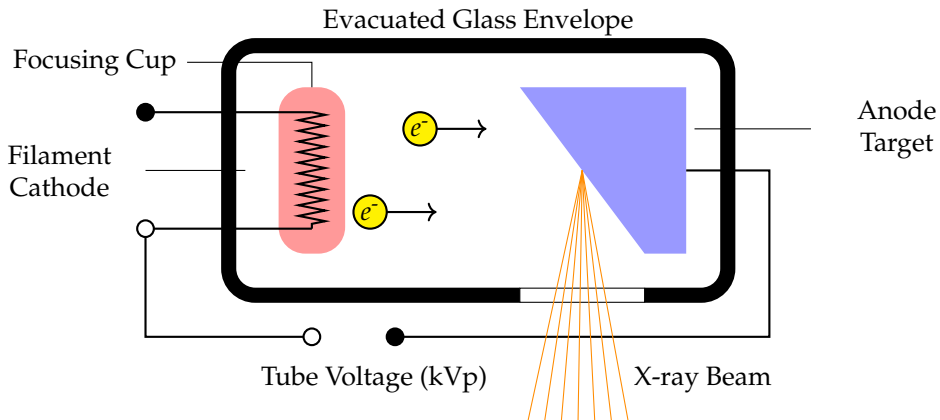


FIGURE 6.2: Schematic of an X-ray tube.

### 6.1.1 Photon Generation

To capture this randomness, Monte Carlo methods are employed. In such simulations, random numbers—typically sampled uniformly from the interval  $[0, 1]$  are transformed into physically meaningful quantities according to the relevant probability distributions. This probabilistic modeling enables realistic simulation of photon transport and forms the basis for the analyses presented in this thesis.

The key components are:

- **Filament (Cathode):** A tungsten wire filament serves as the electron source through thermionic emission. When a current of approximately  $3\text{-}6 \text{ A}$  passes through it, the filament reaches incandescence, releasing electrons from its surface. These free electrons form a cloud near the cathode until they are accelerated toward the anode by the applied high voltage.
- **Focusing Cup:** The filament is embedded in a negatively charged, nickel-made focusing cup. Its function is to electrostatically shape and direct the electron stream toward the anode's focal spot, thereby influencing the resolution and size of the resulting X-ray beam.
- **Anode Target:** The anode consists of a tungsten target, often embedded in a copper support. Tungsten is used for its high atomic number and melting point, enhancing X-ray production and durability. The copper base improves heat dissipation. Typically, less than 1% of the electron energy is converted into X-rays, with the remainder generating heat that must be effectively managed.
- **Evacuated Glass Envelope:** All components are sealed within a borosilicate glass or metal-ceramic housing evacuated to a low pressure (typically  $10^{-5}$  to  $10^{-7} \text{ hPa}$ ). The vacuum allows unimpeded electron flow and prevents arcing.

The housing is usually immersed in insulating oil to provide thermal and electrical isolation.

When high-energy electrons strike the tungsten target, X-ray photons are produced through two primary mechanisms:

- **Bremsstrahlung (Braking Radiation):** This accounts for approximately 80% of X-ray production. When electrons pass close to tungsten nuclei, they are decelerated by the electrostatic attraction, causing them to lose kinetic energy that is emitted as X-ray photons. This process produces a continuous spectrum of X-ray energies from near zero up to the maximum electron energy.
- **Characteristic Radiation:** This occurs when high-energy electrons knock inner shell electrons from tungsten atoms. When outer shell electrons drop down to fill these vacancies, they emit X-rays with discrete, characteristic energies specific to tungsten. Therefore peaks are occurring at the difference of the binding energies of the electron shells. For reference, the atomic model of tungsten is given in Figure 6.7 and the approximate binding energies of the electron shells in Table 6.1.

Shell / Subshell	Binding Energy (keV)
K	69.5
L <sub>1</sub>	12.1
L <sub>2</sub>	11.5
L <sub>3</sub>	10.2
M <sub>1</sub>	2.82
M <sub>2</sub>	2.30
M <sub>3</sub>	2.15
N <sub>1</sub>	0.43
N <sub>2</sub>	0.32
N <sub>3</sub>	0.22

TABLE 6.1: Approximate Electron Binding Energies of Tungsten (W, Z = 74)

In Table 6.1 only binding energies of the K, L and M shells are given, since these are the most relevant for X-ray production. The binding energies of the N shell and higher shells are negligible in this context due to their low binding energies.

Although it is not necessary to understand every technical detail of the X-ray apparatus for the purposes of simulation, I found it important to briefly present the fundamental working principles of the X-ray tube. This background allows one to appreciate how key simulation parameters for photon generation - specifically the tube voltage and the cathode material - influence the resulting X-ray spectrum and photon behavior.

Figure 6.4 below shows an resulting energy spectrum for an X-ray tube with a tungsten cathode operated at 100 kVp. It illustrates the resulting distribution of photon energies, which is shaped by both the material and the applied voltage. The intensity of the different photon energies is measured in *spectral fluence* in  $\text{cm}^{-2} \text{ keV}^{-1}$ ,

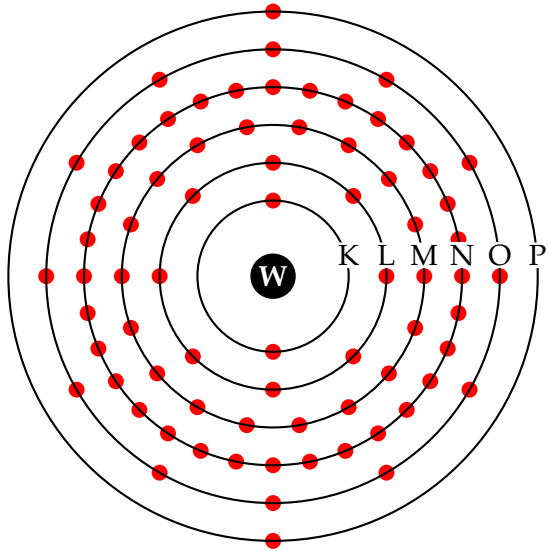


FIGURE 6.3: Bohr model of the tungsten atom ( $W, Z = 74$ ) with electron shells and subshells.

which describes the number of X-ray photons per unit area per unit energy interval. It certainly shows the two components of the X-ray spectrum: the continuous bremsstrahlung spectrum and the characteristic radiation peaks:

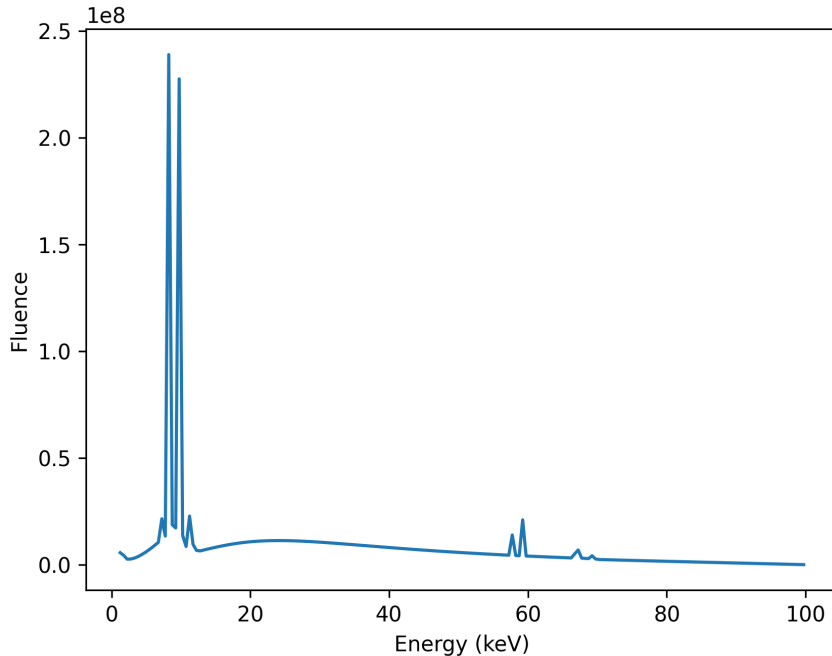


FIGURE 6.4: X-ray spectrum for a tungsten cathode at 100 kVp showing the continuous bremsstrahlung spectrum and characteristic peaks. Build with *SpekPy* [4]

### 6.1.2 Filter

Low energy X-ray photons contribute little to image formation but significantly increase patient dose. Therefore, X-ray tubes are often equipped with filters to selectively attenuate these low-energy photons while allowing higher-energy photons to pass through. This process, known as beam hardening, improves image quality by reducing scatter and enhancing contrast. Common filter materials include aluminum, copper, and molybdenum, which are chosen based on their atomic number and thickness to effectively absorb low-energy photons while minimizing the impact on higher-energy photons [5].

As can be seen in Figure 6.5, the filter is placed at the X-ray tube margin such that the photons hit the filter after the anode target and before leaving the X-ray tube. Followingly X-rays pass through the filter before reaching the patient.

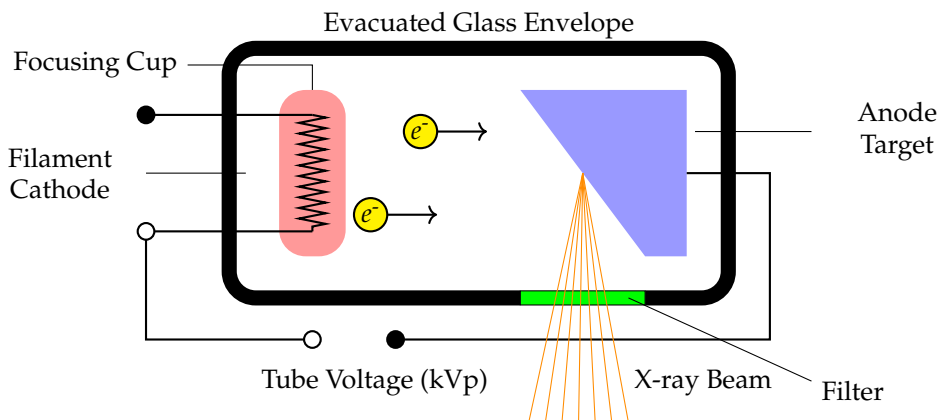


FIGURE 6.5: Schematic of an X-ray tube with Filter.

Throughout this thesis, a filter consisting of 0.4 mm Tin (Sn) and 0.1 mm Copper (Cu) is used for the simulations. This filter is chosen to represent a realistic X-ray tube filter that is commonly used in clinical practice [8]. The resulting spectrum is shown in Figure 6.6.

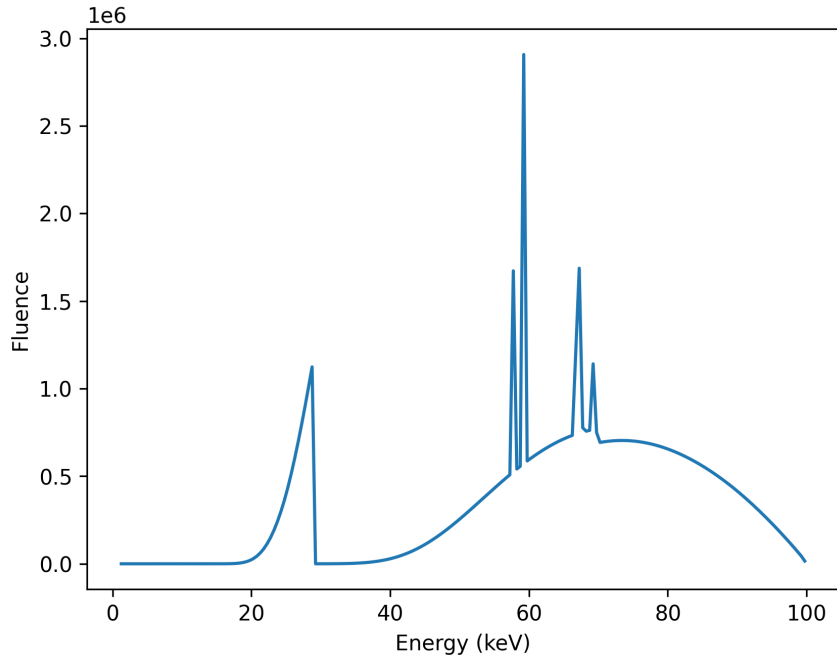


FIGURE 6.6: X-ray spectrum for a tungsten cathode at 100 kVp with a 0.4 mm showing the continuous bremsstrahlung spectrum and characteristic peaks. Build with *SpekPy* [4]

## 6.2 Photon Generation

In the context of Monte Carlo simulations, photons are generated from the X-ray tube source, which is typically modeled as a point source emitting photons within a conical beam. The emission cone is defined by a half-angle  $\Theta$ , which determines the angular distribution of emitted photons. – The emitted photons are characterized by two key properties: their direction and energy.

### Photon Energy

The photon energy is sampled from the X-ray tube spectrum as described in Section 6.1.2. In the simulations referenced in this thesis the spectra are generated utilizing *SpekPy* [4, 6]. The energies of the resulting photons are sampled via inverse transform sampling from the normalized spectrum.

Inverse transform sampling [3] is a method to generate random samples from a target distribution using uniformly distributed random variables, such as those generated by a Quasi-Monte Carlo sequence.

**Definition 6.2.1** (Inverse Transform Sampling).

Let  $F_X : \mathbb{R} \rightarrow [0, 1]$  be the cumulative distribution function (CDF) of a continuous, strictly increasing random variable  $X$ . The method of *inverse transform sampling* generates a realization of  $X$  by the following procedure:

1. Generate a sample  $U$  from the uniform distribution on the unit interval, i.e.,  $U \sim \mathcal{U}(0, 1)$ .

2. Compute the value  $X := F_X^{-1}(U)$ , where  $F_X^{-1}$  denotes the inverse of the CDF  $F_X$ .

**Theorem 6.2.2.**

Let  $F_X$  be a continuous and strictly increasing cumulative distribution function, and let  $U \sim \mathcal{U}(0, 1)$ . Then the random variable

$$X := F_X^{-1}(U)$$

has cumulative distribution function  $F_X$ , i.e.,

$$\mathbb{P}(X \leq x) = F_X(x), \quad \text{for all } x \in \mathbb{R}.$$

*Proof.*

Since  $F_X$  is continuous and strictly increasing, its inverse  $F_X^{-1}$  exists. For any  $x \in \mathbb{R}$ , we compute:

$$\mathbb{P}(X \leq x) = \mathbb{P}(F_X^{-1}(U) \leq x) = \mathbb{P}(U \leq F_X(x)) \stackrel{\substack{\text{since } F_X \text{ is strictly} \\ \text{decreasing}}}{=} F_X(x),$$

because  $U \sim \mathcal{U}(0, 1)$  and thus  $\mathbb{P}(U \leq u) = u$  for all  $u \in [0, 1]$ . This shows that  $X$  has CDF  $F_X$ .  $\square$

### Photon Direction

The direction of each emitted photon is sampled uniformly within a conical emission cone defined by the half-angle  $\Theta$ . For the simulation a spherical alignment of the X-ray tube is assumed, such that the beam is oriented along the vector  $\vec{v} = (v_1, v_2, v_3)$  in the Cartesian coordinate system.

Followingly, the direction of the emitted photon is sampled based on two random values  $u_1, u_2 \in [0, 1)$  as follows:

1. Sample a random angle  $\theta$  uniformly from the interval  $[0, \Theta]$  with  $u_1$ :

$$\theta = u_1 \cdot \Theta$$

2. Sample a random azimuthal angle  $\phi$  uniformly from the interval  $[0, 2\pi)$  with  $u_2$ :

$$\phi = u_2 \cdot 2\pi$$

3. Compute the direction vector  $\vec{d}$  of the photon as:

$$\vec{d} = (\sin(\theta) \cos(\phi), \sin(\theta) \sin(\phi), \cos(\theta))$$

## 6.3 Scattering and Attenuation

This section provides the basic concepts of photon interaction with matter. The interaction relevant for medical imaging results in a reduction of radiation intensity, which corresponds to a decreased number of photons reaching the detector. Hereby X-ray photons may be fully absorbed by *photoelectric absorption* or undergo either

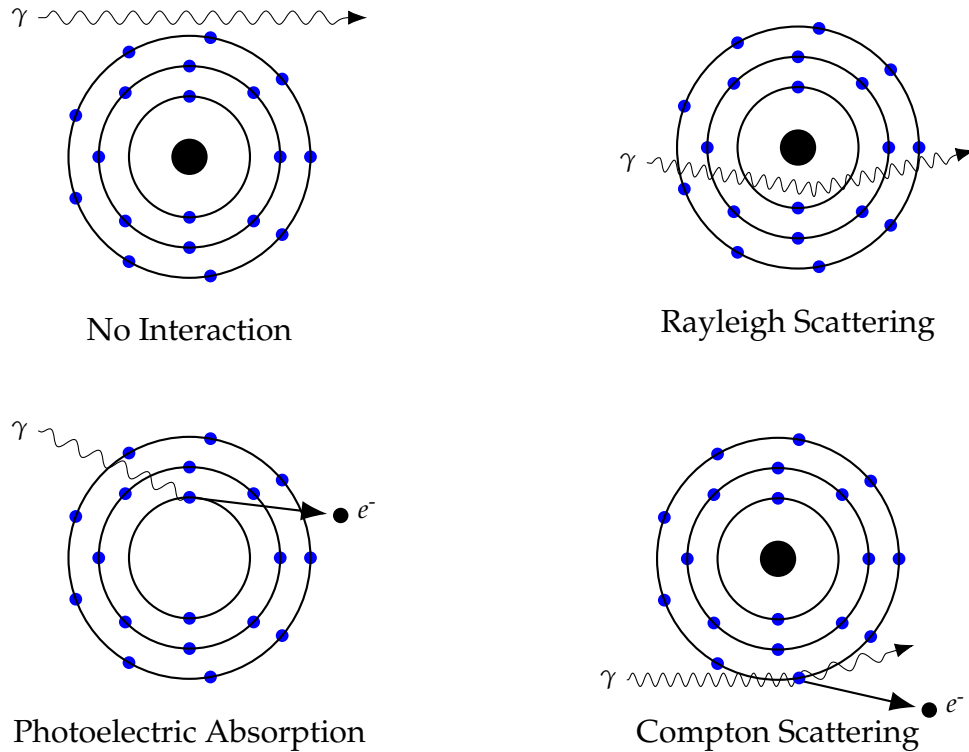


FIGURE 6.7: Principles from photon interaction with matter similar to [2, Chap. 7]

*elastic scattering* (Rayleigh) or *inelastic scattering* (Compton) as they interact with matter.

The attenuation of X-ray photons arises from physical processes that alter their number, direction, or energy as they interact with matter. These interactions occur at the level of individual photons and are highly dependent on the photon energy. This section presents an overview of the primary interaction mechanisms relevant to attenuation like in [2].

For correctness, in the simulations it is further assumed that the X-ray photons are propagating through vacuum before entering and after exiting the phantom. Usually the tissues are surrounded by air, which has a negligible effect on the photon transport.

### 6.3.1 Free Path Length

All mentioned interaction processes - the photoelectric effect, Compton scattering and Rayleigh scattering - are probabilistic in nature. The according attenuation coefficients  $\mu$  characterizes the extend of the beam being reduced by its according effect, when passing through the material, in  $\text{cm}^2 \text{g}^{-1}$ . For the simulation of photons, the attenuation coefficients are dependent on the according energy  $E$  of the photon and the material at spherical location  $x$  of the photon. The coefficients are summarized in Table 6.2.

Interaction Type	Attenuation Coefficient
Photoelectric Effect	$\mu_{\text{PE}}(x, E)$
Rayleigh Scattering	$\mu_{\text{RS}}(x, E)$
Compton Scattering	$\mu_{\text{CS}}(x, E)$

TABLE 6.2: Attenuation coefficients for different photon interaction mechanisms.

The linear attenuation coefficient  $\mu(x, E)$  is the sum of the individual attenuation coefficients of the interaction coefficients:

$$\mu(x, E) = \mu_{\text{PE}}(x, E) + \mu_{\text{RS}}(x, E) + \mu_{\text{CS}}(x, E)$$

When an X-ray photon enters the phantom two main effects are considered:

- **Attenuation:** The photon may be absorbed or Scattered.
- **No Interaction:** The photon may pass through the phantom without any interaction.

The *free path length*  $t$  of a photon describes the distance a photon takes to traverse through the phantom before it interacts with matter. Supposing the phantom's location is  $x$  and the photon is traveling in the unit direction  $\vec{v}$ , as in [1] the free path length  $t$  follows the distribution given by:

$$t \sim \mu(x, E) \exp \left[ - \int_0^t \mu(x + s \cdot \vec{v}) \right]$$

Check: nach dem paper müsste  $\mu$  abhängig vom Endpunkt sein.

The free path length  $t$  is constrained by the maximum distance  $c$  ( $0 \leq t \leq c$ ) to the next exit point of the phantom along the ray with direction  $\vec{v}$ . After leaving the phantom, we assume the photon is reaching the detector or leaving the simulation domain.

The probability of the photon to leave the phantom unaltered is described by the *escape probability*  $\mathcal{P}$  of a photon at a given position  $A$  with unit direction  $\vec{v}$  and energy  $E$  as in [1]:

$$\mathcal{P}(x, \vec{v}, E) = \exp \left[ - \int_0^c \mu(x + t\vec{v}, E) dt \right],$$

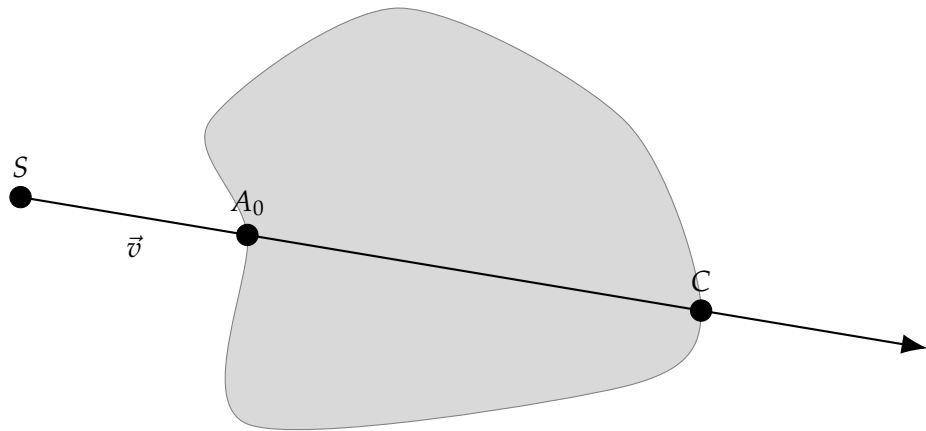


FIGURE 6.8: Illustration of the entry and exit point of the ray of a photon without interaction.

**Todo:** Image illustrating the entry and exit point of a ray without interaction.

### 6.3.2 Compton Scattering

*Compton scattering* is the most dominant interaction mechanism for X-ray photons in tissue [2, Chap. 7]. It occurs when a X-ray photon with considerably higher energy than the binding energy of an outer shell electron collides with this electron. This interaction results in a transfer of energy and momentum. The electron is ejected from the atom, while the incoming photon is scattered at an angle and its energy is reduced.

A portion of the incident photon energy is transferred to the electron, which is referred to as the "recoil electron" or Compton electron. The interaction produces a positive ion, the "recoil electron" and a scattered photon. If the deflection angle of the scattered photon is small, most of the energy is retained by the scattered photon. The deflection angle can vary from 0 to 180 degrees, depending on the energy transfer during the interaction.

### 6.3.3 Rayleigh Scattering

*Rayleigh scattering* is a type of elastic scattering that occurs at low X-ray energies [2, Chap. 7]. The incident photon interacts with several electrons that are usually bound in the outer shells of the atom. In this process, the low energy photon is not ejected, but rather the electrons and in turn the whole atom is set to vibration with respect to the incident photon's wavelength. The vibrating photon transfers its excess energy to an electromagnetic photon with the same wavelength but probably a different direction than the incident photon. The majority of these scattered photons are emitted in a forward direction. This interaction does not result in the ejection of electrons from the atom, and no ionization occurs as no energy is converted into kinetic energy.

Although Rayleigh scattering is taking place in the X-ray tube, it can be excluded from the linear attenuation coefficient, as it does not contribute to the attenuation of the X-ray beam in the same way as Compton scattering or photoelectric absorption. As described in [5], the exclusion of Rayleigh scattering from the linear attenuation

coefficient is based on the assumption that the characteristic radiation emitted by the target is isotropic, meaning it is emitted uniformly in all directions. As the X-ray is not attenuated by Rayleigh scattering, it is a common assumption to exclude Rayleigh scattering from the attenuation coefficient.



## Chapter 7

# The Simulation Algorithm

In this chapter the implementation algorithm is presented. The algorithm takes elements from the gQMCFD algorithm from [1] and adapts it to the needs of this thesis. The algorithm is designed to simulate X-ray images efficiently, including scattering effects and is specifically tailored to analyze and compare the performance of different sampling methods.

Forced Fixed Detection (**FFD**) is a method used to simulate X-ray images efficiently, particularly in the context of X-ray imaging systems. It is designed to handle multiple scatter orders and can be used either with Monte Carlo sequences or with Quasi-Monte Carlo (QMC) sequences for sampling the random variables involved in the simulation

### 7.1 Algorithm overview

### 7.2 Sub-Algorithms

To structure the algorithms into the different physical effects, this section is gathering highly relevant algorithms which are later orchestrated by the main simulation algorithm.

#### 7.2.1 Photon Generation

For the photon generation, two main properties for each photon do need to be sampled:

- The *Photon Energy* which is sampled with one random variable from the spectrum.
- The *Photon Direction* which is sampled with two random variables uniformly in the cone of the beam with direction  $d$  and angle  $\alpha$ .

For the photon energy the spectrum of the X-ray tube is referenced with an array of energies and another array with the according fluence. These spectrum values are sampled with *Spekpy* [4, 6] for a X-ray tube with the following parameters:

- **Tube Voltage:** 120 kV
- **Anode Material:** Tungsten
- **Filtration:** 0.4 mm of Tin (Sn) and 0.1 mm of Copper (Cu)

- **Target Angle:**  $12.5^\circ$

The following algorithm samples the photon energy from the spectrum using inverse transform sampling. The algorithm takes an array of energies and their corresponding fluence values, normalizes the fluence to create a probability density function (PDF), computes the cumulative distribution function (CDF) and then uses a random variable to sample the photon energy based on the CDF.

---

**Algorithm 1** Photon Energy Sampling from Spectrum

---

**Require:** Array of energies  $E = [E_1, E_2, \dots, E_n]$   
**Require:** Corresponding fluence values  $\Phi = [\phi_1, \phi_2, \dots, \phi_n]$   
**Require:** Number of samples  $N$   
**Require:** Random variable  $u \sim \mathcal{U}(0, 1)$   
**Ensure:** Sampled photon energies  $S = [s_1, s_2, \dots, s_N]$

// Normalize fluence values:

- 1: 
$$T \leftarrow \sum_{i=1}^n \phi_i$$
- 2: 
$$\text{PDF}[i] \leftarrow \frac{\phi_i}{T}$$
- 3: // Compute cumulative distribution function:
- 4: **for**  $i = 2$  to  $n$  **do**
- 5:      $\text{CDF}[i] \leftarrow \text{CDF}[i - 1] + \text{PDF}[i]$
- 6: **end for**
- // Note:  $\text{PDF}[i] > 0$  in the spectrum, therefore CDF is strictly increasing.
- 7: Create interpolating function  $\text{InverseCDF}(u)$  from  $(\text{CDF}[i], E[i])$
- 8: **return**  $\text{InverseCDF}(u)$

---

Further the photon direction is sampled uniformly in the cone with angle  $\alpha$  of the beam of the X-ray tube with spherical direction  $\vec{d}$ . Therefore two random variables are required  $u_1, u_2 \sim \mathcal{U}(0, 1)$ .

**Algorithm 2** Uniform Direction Sampling Within a Cone

---

**Require:** Cone angle  $\alpha$   
**Require:** Unit beam direction vector  $\vec{d} = (d_1, d_2, d_3)$   
**Require:** Random variables  $u_1, u_2 \sim \mathcal{U}(0, 1)$   
**Ensure:** Sampled direction vector  $\vec{v}$  uniformly within cone around  $\vec{d}$

// Calculate angles according to samples

- 1:  $\theta \leftarrow \arccos(1 - u_1(1 - \cos \alpha))$  // Polar angle
- 2:  $\phi \leftarrow 2\pi u_2$  // Azimuthal angle
- 3: // Calculate local direction vector in spherical coordinates

$$\vec{v}_{\text{local}} \leftarrow \begin{pmatrix} \sin \theta \cos \phi \\ \sin \theta \sin \phi \\ \cos \theta \end{pmatrix}$$

// Orthonormal basis construction (Gram-Schmidt)

- 4:  $\vec{w} \leftarrow \vec{d}/\|\vec{d}\|$  // Normalized cone axis
- 5: **if**  $|w_3| < 0.999$  **then**
- 6:    $\vec{a} \leftarrow (0, 0, 1)$
- 7: **else**
- 8:    $\vec{a} \leftarrow (1, 0, 0)$
- 9: **end if**
- 10:  $\vec{u} \leftarrow \frac{\vec{a} \times \vec{w}}{\|\vec{a} \times \vec{w}\|}$  // Orthogonal vector
- 11:  $\vec{v} \leftarrow \vec{w} \times \vec{u}$  // Complete right-handed basis
- 12: // Rotate local vector into global coordinates
- 13:  $\vec{v}_{\text{global}} \leftarrow \vec{u}(\vec{v}_{\text{local}})_x + \vec{v}(\vec{v}_{\text{local}})_y + \vec{w}(\vec{v}_{\text{local}})_z$
- 14: **return**  $\vec{v}_{\text{global}}$

---

In this section the gQMCFD algorithm from [1] is introduced. The gQMCFD algorithm uses QMC methods to simulate an X-ray image efficiently including scattering effects. The algorithm is designed to handle multiple scatter orders and utilizes In this section the Algorithm 3 from [1] is presented. The **QMC**-Method is used to simulate the X-ray image. Therefore the algorithm is used The following pseudoalgorithm outlines the process of simulating X-ray photon transport using Quasi-Monte Carlo (QMC) methods. The algorithm generates a sequence of QMC samples to determine the initial positions and directions of photons, simulates their transport through a defined geometry, and records the results of interactions with materials. By that many other algorithms are used such als the Rational Inverse Transform with Aliasing (**RITA**) algorithm.

**Algorithm 3** gQMCFFD: X-ray Scatter Simulation (Part 1)

## gQMCFFD

1: **Input:** Max. scatter order  $N$ , phantom geometry  $\mathcal{P}$ , energy spectrum  $\phi$ , beam angle  $\alpha$ , set of detector pixels  $\mathcal{G} = \{G_1, \dots, G_s\}$ , QMC point  $u^j \in [0, 1]^{4N}$ , step size  $\Delta s$

2: **Initialize photon using**  $u_1^j, u_2^j, u_3^j$ :

- energy  $E_0 \sim \phi(E)$  by inverse transform sampling with  $u_1^j$
- direction  $\vec{\omega}_0$  within cone angle  $\alpha$  using  $u_2^j, u_3^j$
- weight  $W_0 = I_0(\vec{\omega}_0) = 1$
- escape probability  $p_0 = 0$  **TODO: ist das richtig initialisiert?**

3: Compute entry point: find smallest  $t_0$  s.t.  $A_0 = S + t_0 \cdot \vec{\omega}_0 \in \partial \mathcal{P}$

4: Initialize:  $f_{n,k} = 0$  for all  $D_k \in \mathcal{G}$

5: **for**  $i = 1$  to  $N$  **do**

6:    $t_i \leftarrow \Delta s$  // Initialize path length

7:    $A_i \leftarrow A_{i-1} + t_i \cdot \vec{\omega}_{i-1}$  // Initialize position

8:   **while**  $A_i \in \mathcal{P}$  **and**  $\int_0^{t_i} \mu_{\text{tot}}(A_{i-1} + s\vec{\omega}_{i-1}, E_{i-1}) ds < -\ln(1 - (1 - p_{i-1})u_{4i}^j)$  **do**

9:      $t_i \leftarrow t_i + \Delta s$  // Update path length

10:     $A_i \leftarrow A_{i-1} + t_i \cdot \vec{\omega}_{i-1}$  // Update position

11: **end while**

12:   **// Sample interaction type**

13:   **if**  $\mu_{\text{tot}}(A_i, E_i) \cdot u_{4i+3}^j < \mu_{\text{comp}}(A_i, E_i)$  **then**

14:      $\delta^i = 0 \rightarrow \text{Compton Scattering}$

15:      $p_{y0}$  gemäß Gleichung (5)

16:      $\vec{\omega}_i \leftarrow \text{comptonDirectionSampling}(E_{i-1}, \vec{\omega}_{i-1}, u_{4i+1}^j, u_{4i+2}^j)$

17:   **else if**  $\mu_{\text{comp}}(A_i, E_i) \leq \mu_{\text{tot}}(A_i, E_i) \cdot u_{4i+3}^j < \mu_{\text{comp}}(A_i, E_i) + \mu_{\text{ray}}(A_i, E_i)$  **then**

18:      $\delta^i = 1 \rightarrow \text{Rayleigh Scattering}$

19:      $p_{y1}$  gemäß Gleichung (6)

20:   **else**

21:     **Photoelectric Absorption**  $\rightarrow$  **break**

22:   **end if**

23:   Sample new direction  $\vec{\omega}_i$  using RITA using randoms  $u_{4i+1}^j, u_{4i+2}^j$   
**TODO: herausfinden, wie neue Energie berechnet wird**

24:   Compute escape probability along  $\vec{\omega}_{i-1}$ :

$$p_{i-1} = \exp \left( - \int_0^{c_{i-1}} \mu_{\text{tot}}(A_{i-1} + s\vec{\omega}_{i-1}, E_{i-1}) ds \right)$$

25:   Update weight:  $W_i = W_{i-1} \cdot (1 - p_{i-1})$

26:   **for** each detector pixel  $D_j \in \mathcal{G}$  **do**

27:     Determine forced direction  $\vec{\omega}_{i,j}$  from  $A_i \rightarrow D_j$

28:     Compute transmission factor:

$$T_{i,j} = \exp \left( - \int_0^{b_{i,j}} \mu_{\text{tot}}(A_i + s\vec{\omega}_{i,j}, E_i) ds \right)$$

29:     Compute directional scatter PDF:  $p^y(A_i, E_{i-1} \rightarrow E_i, \vec{\omega}_{i-1} \rightarrow \vec{\omega}_{i,j})$

30:     Update scatter contribution:

$$f_{n,j} += W_i \cdot p^y \cdot T_{i,j}$$

31:   **end for**

32: **end for**

---

**Algorithm 4** gQMCFD: X-ray Scatter Simulation (Part 2)

---

33: **Primary intensity (if unscattered):**  
 34: **for** each detector pixel  $D_j \in \mathcal{G}$  **do**  
 35:     Determine direct line  $\vec{\omega}_{0,j}$  from  $A_0$  to  $D_j$   
 36:     Compute:  

$$T_{0,j} = \exp \left( - \int_0^{b_{0,j}} \mu_{\text{tot}}(A_0 + s\vec{\omega}_{0,j}, E_0) ds \right)$$
  
 37:     Add primary contribution:  

$$f_{n,j} += W_0 \cdot T_{0,j}$$
  
 38: **end for**  
 39: **Output:**  $f_{n,j}$  for each detector pixel  $D_j \in \mathcal{G}$ 


---

## Appendix A

# Frequently Asked Questions

### A.1 How do I change the colors of links?

The color of links can be changed to your liking using:

```
\hypersetup{urlcolor=red}, or  
\hypersetup{citecolor=green}, or  
\hypersetup{allcolor=blue}.
```

If you want to completely hide the links, you can use:

```
\hypersetup{allcolors=.}, or even better:  
\hypersetup{hidelinks}.
```

If you want to have obvious links in the PDF but not the printed text, use:

```
\hypersetup{colorlinks=false}.
```



# Bibliography

- [1] Guiyuan Lin, Shiwo Deng, and Xiaoqun Wang. "An efficient quasi-Monte Carlo method with forced fixed detection for photon scatter simulation in CT". In: *PLOS ONE* 18 (Aug. 2023), e0290266. DOI: [10.1371/journal.pone.0290266](https://doi.org/10.1371/journal.pone.0290266).
- [2] *Medical Imaging Systems : An Introductory Guide*. eng. Image Processing, Computer Vision, Pattern Recognition, and Graphics; 11111. Cham, 2018. Chap. 7,8. ISBN: 9783319965208.
- [3] Thomas Müller-Gronbach, Erich Novak, and Klaus Ritter. *Monte Carlo-Algorithmen*. Springer-Verlag, 2012.
- [4] Gavin Poludniowski. *SpekPy: Python package for simulating X-ray spectra*. Version 2.0.13. 8.08.2024. URL: <https://bitbucket.org/caxtus/book/src/master/>.
- [5] Gavin Poludniowski, Artur Omar, and Pedro Andreo. *Calculating X-ray Tube Spectra: Analytical and Monte Carlo Approaches*. CRC Press, 2022.
- [6] Gavin Poludniowski et al. "SpekPy v2.0—a software toolkit for modeling x-ray tube spectra". In: *Medical Physics* 48.7 (2021), pp. 3630–3637.
- [7] A. Sisniega et al. "Automatic Monte-Carlo Based Scatter Correction For X-ray cone-beam CT using general purpose graphic processing units (GP-GPU): A feasibility study". In: *2011 IEEE Nuclear Science Symposium Conference Record*. 2011, pp. 3705–3709. DOI: [10.1109/NSSMIC.2011.6153699](https://doi.org/10.1109/NSSMIC.2011.6153699).
- [8] Jörg Steidel et al. "Dose reduction potential in diagnostic single energy CT through patient-specific prefilters and a wider range of tube voltages". In: *Medical physics* 49.1 (2022), pp. 93–106.